27

Diamondoids Under Pressure

Sulgiye Park[1], Yu Lin[2], and Wendy L. Mao[1,3]

ABSTRACT

Due to their outstanding properties, diverse geometry, and ability to be manipulated and functionalized, diamondoids have gained interest as highly attractive targets as molecular building blocks for applications in biomedicine, materials science, and nanotechnology, in addition to the field of petroleum engineering (Clay et al., 2009; Mcintosh et al., 2004; Sasagawa & Shen, 2008; Willey et al., 2006; Zhang et al., 2016). Diamondoid molecules are also a useful system for basic science studies. They display atomic-level uniformity and a systematic series of sizes and geometries, making them ideal materials for exploring how different parameters can be used to tune properties. In this chapter, the pressure-induced structural modifications in a range of diamondoids are reported. In section 27.2, the critical role of molecular geometry in determining the phase transition pressures and bulk moduli of diamondoids is discussed, followed by the sensitivity of diamondoids to hydrostaticity and deviatoric stress under compression. Section 27.3 examines recent work investigating functionalized diamondoids at high pressure and concludes with a perspective for future work and exciting potential directions for studying diamondoids at extreme conditions.

27.1. INTRODUCTION

Carbon-based nanomaterials, such as graphene, fullerenes, and carbon nanotubes, have attracted broad interest in both science and industry for their unique and outstanding properties, which make them attractive for a wide range of nanotechnology applications (Stauss & Terashima, 2017; Yang et al., 2016). Here, another exceptional member in the carbon nanomaterial family, diamondoid molecules and their functionalized derivatives, are discussed in terms of how their structures and properties evolve under extreme conditions.

Diamondoid molecules are hydrogen-terminated carbon nanomaterials in the form of $C_{4n+6}H_{4n+12}$ (Mansoori, 2008; Marchand, 2003). With size variations of 0.5–2 nm in diameter, diamondoids represent the ultimate limit in reducing the size of diamond. The most basic unit of diamondoids, adamantane ($C_{10}H_{16}$), is composed of ten-carbon atoms which form a tetra-cyclic cage that can be superimposed on a cubic diamond lattice, with larger diamondoids consisting of varying numbers of these cage units (Figure 27.1a). The lower diamondoids, ada-, dia- and tria-mantane (when $n \leq 3$), each have one isomer. Higher diamondoids (when $n > 3$) have multiple structural isomers depending on the relative directions of face-fused single cage adamantane units (Clay et al., 2009; Mcintosh et al., 2004; Sasagawa & Shen, 2008; Willey et al., 2006; Zhang et al., 2016). Entirely constituted by sp^3-bonded carbons arranged in a three-dimensional (3D) network with covalent interatomic interactions, diamondoid molecules are highly stable and dense. Their resemblance to bulk diamond means that diamondoids similarly have high thermal stability and rigidity.

In nature, diamondoid molecules can be found in deep fossil fuel reservoirs, such as coal, petroleum, gas condensate, and natural gas, formed by hydrocarbon rearrangement reactions under acidic conditions (Fort & Schleyer

[1] *Department of Geological Sciences, Stanford University, Stanford, California, USA*

[2] *Stanford Institute for Materials and Energy Sciences, SLAC National Accelerator Laboratory, Menlo Park, California, USA*

[3] *Photon Science, SLAC National Accelerator Laboratory, Menlo Park, California, USA*

Carbon in Earth's Interior, Geophysical Monograph 249, First Edition. Edited by Craig E. Manning, Jung-Fu Lin, and Wendy L. Mao.

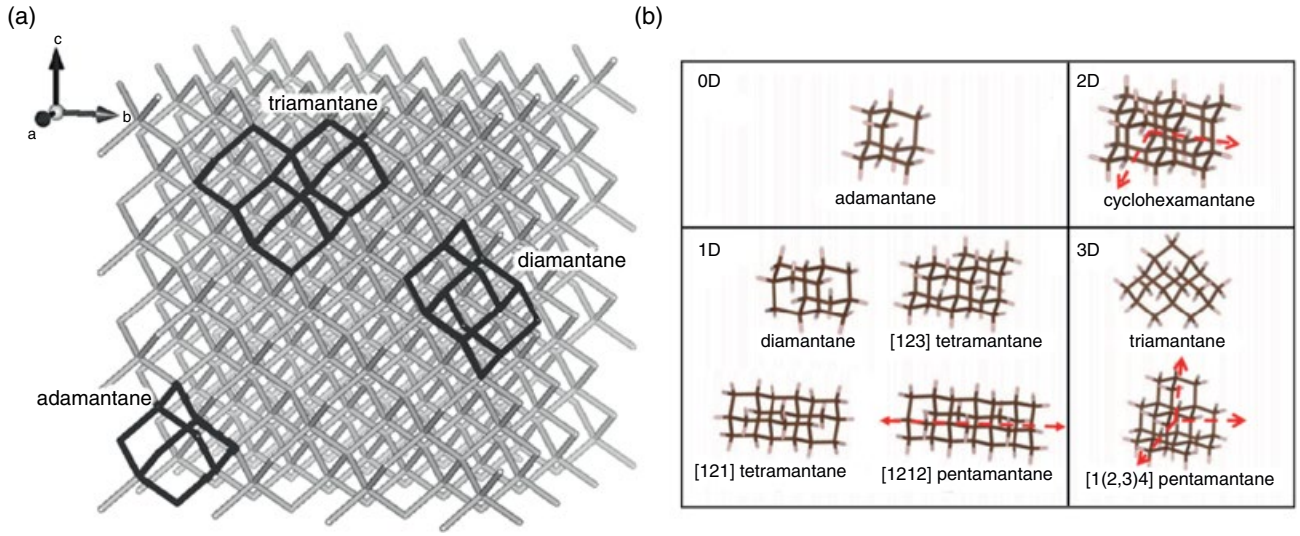

Figure 27.1 (a) Molecular structure of lower diamondoids superimposed on a cubic diamond lattice. (b) Molecular structures of the eight diamondoids studied; relative directions of face-fused adamantane cages in polymantane homologues are indicated by dashed arrows. (Adapted from Yang et al., 2016.) See electronic version for color representation of the figures in this book.

1964; Katz et al., 2008). Due to their similarity to the bulk diamond structure, diamondoids are extremely resistant to weathering, which enables them to be isolated from petroleum by hydrocracking oil to gas (Dahl et al., 2010; Ma, 2016; Ma et al., 2017; Stout & Douglas, 2004). Bulk concentration of the petroleum diamondoids is adamantane, which is generally accompanied by small amounts of diamantane and triamantane (Katz et al., 2008; Mckervey, 1980; Wingert, 1992). Higher diamondoids also exist in minute quantities in a gas condensate produced from very deep (~6.8 km below the Earth's surface) petroleum reservoirs (Dahl et al., 2003; R. Lin & Wilk, 1995). Diamondoids represent an important geochemical tool for characterizing reservoir fluids. Applied solely and/or in conjunction with well-known biomarkers, diamondoids are used for correlation, biodegradation, and maturity assessments involved in petroleum exploration, quality evaluation, and chemical fingerprinting of light petroleum and gasoline (Ekweozor & Telnaes, 1990; Mackenzie et al., 1980; Requejo et al., 1992; Seifert & Moldowan, 1986; Van Graas, 1990). For example, by taking advantage of the rigidity and concentration effect of diamondoids, one can reliability constrain the extent of thermal cracking and the depth at which it occurs in a given reservoir (Dahl et al., 1999).

Due to their outstanding properties, diverse geometry, and ability to be manipulated and functionalized, diamondoids have gained interest as highly attractive targets as molecular building blocks for applications in biomedicine, materials science, and nanotechnology, in addition to the field of petroleum engineering (Clay et al., 2009; Mcintosh et al., 2004; Sasagawa & Shen, 2008; Willey et al., 2006; Zhang et al., 2016). Furthermore, diamondoid molecules are a useful system for basic science studies. They display atomic-level uniformity and a systematic series of sizes and geometries, making them ideal materials for exploring how structural and chemical parameters affect properties.

In this chapter, the pressure-induced structural modifications in a range of diamondoids are reported. In section 27.2, the critical role of molecular geometry in determining the phase transition pressures and bulk moduli of diamondoids is discussed, followed by the sensitivity of diamondoids to hydrostaticity and deviatoric stress under compression. Section 27.3 examines recent work investigating functionalized diamondoids at high pressure, followed by a conclusion on perspective for future work and exciting potential directions for studying diamondoids at extreme conditions.

27.2. ROLE OF MOLECULAR GEOMETRY ON DIAMONDOIDS AT HIGH PRESSURE

The high-pressure behavior of carbon allotropes has long been a subject of intense investigation, fueled by the dramatic changes in physical and chemical properties at extreme conditions. Diamondoids exhibit interesting structural stability coupled with configurational changes in their molecular packing at high pressures. Here we report pressure-induced modifications in eight selected diamondoid crystals with varying molecular geometries: adamantane, diamantane, triamantane, [121]tetramantane, [123]tetramantane, [1212]pentamantane, [1234] pentamantane, and cyclohexamantane (Figure 27.1) (Yang et al., 2016). A summary of the structural

information and physical parameters for the eight diamondoids studied is given in Table 27.1.

To understand the high-pressure behavior of diamondoids, diamond-anvil cell was utilized to reach pressures up to ~40 GPa. Structural evolution as a function of pressure was then probed using both Raman spectroscopy and angle-dispersive synchrotron X-ray powder diffraction (XRD). The XRD results were used to produce pressure-volume curves, which were fit to an isothermal third-order Birch-Murnaghan equation of state (EOS) (Birch, 1947). Pressure was increased incrementally under both hydrostatic and nonhydrostatic conditions, and measurements were collected both during compression and decompression cycles.

At ambient conditions, diamondoid molecules exhibit multiple characteristic vibrational modes, appearing at three different wavenumber ranges: C-C-C bending and C-C stretching at lower Raman shifts ~200–900 cm^{-1}, C-H wagging/C-H_2 twisting/C-H_2 scissoring at midrange Raman shifts ~900–1600 cm^{-1}, and C-H stretching at higher Raman shifts ~2800–3200 cm^{-1} (Filik, 2010; Filik et al., 2006a, 2006b). Upon compression, the only vibrational region undergoing a continuous, monotonic change is the C-C stretching mode, while other vibrational regions display complex peak splitting and merging (Figure 27.2a) (Yang et al., 2016). The C-C stretching region, which blue shifts as a function of pressure, originates from a breathing vibration across a single adamantane cage (Filik et al., 2006a). The pressure-induced change in peak position is attributed to the parabolic relationship from the changes in the C-C bond force constant under compression. In some diamondoid molecules (adamantane, diamantane, and [121]tetramantane), the evolution of this breathing mode at high pressure undergoes an obvious discontinuity, due to the alteration in intermolecular packing, which in turn, modifies the intramolecular vibrations (Figure 27.2b). Despite the discontinuity, however, the breathing mode persists even up to the highest pressure reached, indicating that the diamond-like cages can remain intact even up to high pressures. Upon pressure release, the changes observed in all Raman spectra are completely reversible. The observation provides evidence against the reconstructive mechanisms widely described for other carbon-containing molecular solids, wherein decomposition and amorphization are readily discussed in terms of the breaking and formation of new bonds at high pressures. The comparable pressure range used in our studies to those reported previously for carbon-based solids suggests that only modifications of molecular packing are observed for diamondoids at high pressure due to the particularly rigid diamond-like molecular cages of diamondoids (Yang et al., 2016).

In agreement with the Raman spectroscopy, XRD patterns show a completely reversible trend upon pressure release in all the diamondoids studied. Additionally, strong hysteresis effects are observed upon decompression. As observed in Figure 27.2c, [123]tetramantane with an ambient structure of P1 exhibits a new peak (marked with an asterisk) at a pressure ~11.8 GPa that persists up to ~15 GPa. Upon release, the metastable high-pressure phase remains until pressure is completely reversed, indicating a strong hysteresis effect under hydrostatic condition.

The relative pressure-induced volume changes for the low-pressure phases were fit to a third-order Birch-Murnaghan EOS, and the results are plotted in Figure 27.3. The small ambient bulk moduli (K_0) of all diamondoid crystals are attributed to their weak intermolecular van der Waals interactions, wherein the compression at low pressures occurs through simple volume reduction of the intermolecular spacing. At higher pressures, the volume reduction becomes increasingly difficult due to the dominant Coulomb repulsion and stiff intramolecular covalent bonds, resulting in rapid increase in bulk moduli and large pressure derivatives (K_0') (Yang et al., 2016).

The bulk moduli of the diamondoids illustrate a systematic correlation with their molecular geometry. Zero-dimensional adamantane with all dimensions measured within the nanoscale has the lowest bulk modulus, while 3D [1(2,3)4]pentamantane and 2D cyclohexamantane have the highest bulk moduli (Figure 27.3b). It is interesting to note that 2D cyclohexamantane, which is confined to one dimension at nanoscale, has similar bulk modulus as 3D [1(2,3)4] pentamantane, which resembles bulk nanomaterials that are unconfined to the nanoscale in any dimension. One-dimensional diamondoid molecules that are confined to two (x,y) dimensions fall somewhere in between 0D adamantane and 2D–3D diamondoids. For comparisons, the EOS of C_{60} fullerene falls within a similar region in the pressure-volume space as diamondoid crystals, which can be attributed to its comparable molecular size, geometry, and intermolecular interactions (Yang et al., 2016).

For the pressure range studied, the compressibility of the diamondoid crystals is influenced by the hydrogen interactions between adjacent molecules, which help govern the molecular geometry and packing orientations. As summarized in Table 27.1, a mutual feature across the diamondoid crystals is the fast onset of pressure-induced structural transitions. Except for triamantane, which persists its structure up to ~18 GPa, all other diamondoids undergo at least one structural phase transition. Interestingly, the phase transition pressure in diamondoids is found to be positively correlated to the hydrogen separation distance (H–H distance), or the distance between the nearest hydrogen atoms in adjacent molecules (Yang et al., 2016). The smaller H–H distances, such as those of adamantane (2.37 Å) and [1(2,3)4]pentamantane (2.30 Å), suggest that the adjacent molecules are close and relatively

Table 27.1 Structural information for the eight investigated diamondoid crystals.

Diamondoid	Molecular Formula	Molecular Weight	Molecular Volume (Å^3)	Unit Cell Volume (Å^3)	Density [g/cm^3]	Ambient Phase	Dimensionality	H—H Distance (Å)	K_0 (GPa)	K_0' (GPa)
Adamantane	$C_{10}H_{16}$	136.125	N/A	844	1.08	*Fm3m*	0D	2.37	3.2(0.2)	19(1.0)
Diamantane	$C_{14}H_{20}$	188.314	N/A	1033	1.21	*Pa3*	1D	2.65	5.0(0.6)	19.5(2.8)
Triamantane	$C_{18}H_{24}$	240.390	N/A	5124	1.24	*Fddd*	3D	2.81	13.9(1.6)	9.6(1.5)
[121]tetramantane	$C_{22}H_{28}$	292.466	284	768	1.27	$P2_1/n$	1D	2.53	5.5(0.6)	18.8(2.3)
[123]tetramantane	$C_{22}H_{28}$	292.466	—	369	1.31	*P1*	1D	2.52	5.0(1.3)	20.0(1.1)
[1(2,3)4]pentamantane	$C_{26}H_{32}$	344.542	329	1815	1.26	*Pnma*	3D	2.30	16.0(1.2)	11.8(1.0)
[1212]pentamantane	$C_{26}H_{32}$	344.542	—	1763	1.30	$P2_12_12_1$	1D	2.48	8.1(0.8)	8.5(1.5)
Cyclohexamantane	$C_{26}H_{30}$	342.526	319	1239	1.38	*-R3*	2D	2.63	13.5(1.5)	11.9(1.8)

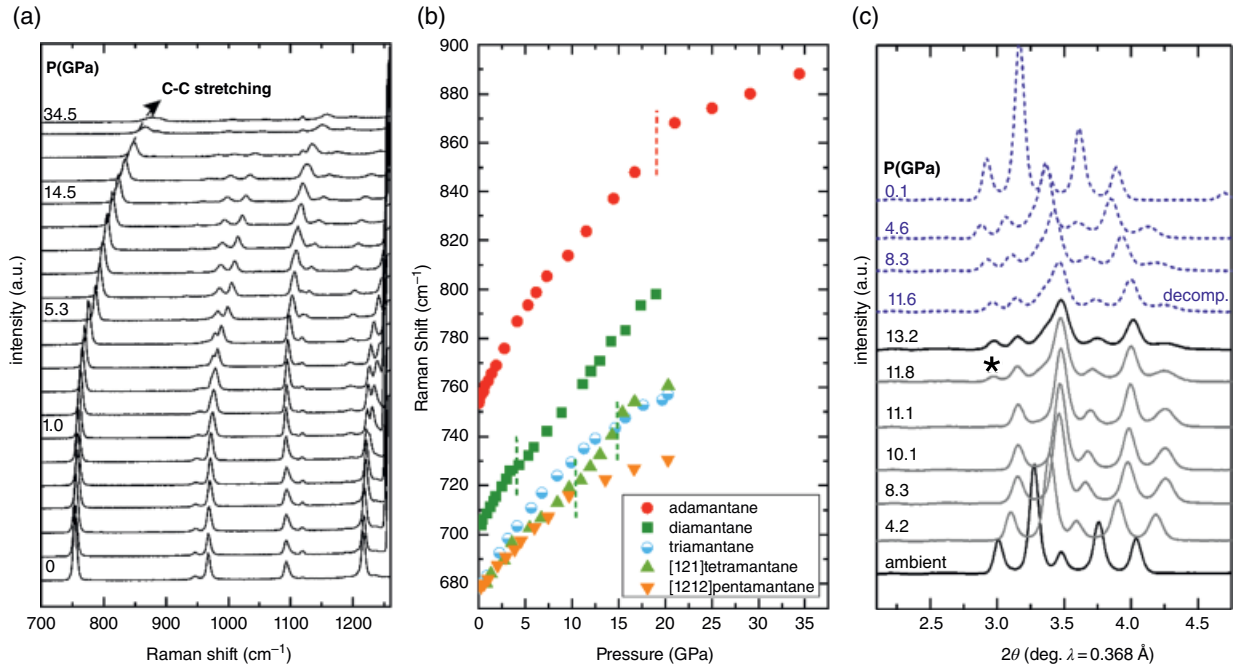

Figure 27.2 (a) Raman spectra of adamantane as a function of increasing pressure. The C-C stretching mode, or the carbon cage breathing vibration, exhibits a smooth shift to higher Raman shift with increasing pressure. (b) Evolution of carbon cage breathing mode for representative diamondoid molecules as a function of increasing pressure. Dashed vertical lines indicate distinctive discontinuities in the development trend of the breathing mode. (c) Representative XRD patterns of [123]tetramantane as a function of compression and decompression (decomp). Asterisk denotes a new peak that indicates a phase transformation. (Parts a and b reproduced from Yang et al., 2016.) See electronic version for color representation of the figures in this book.

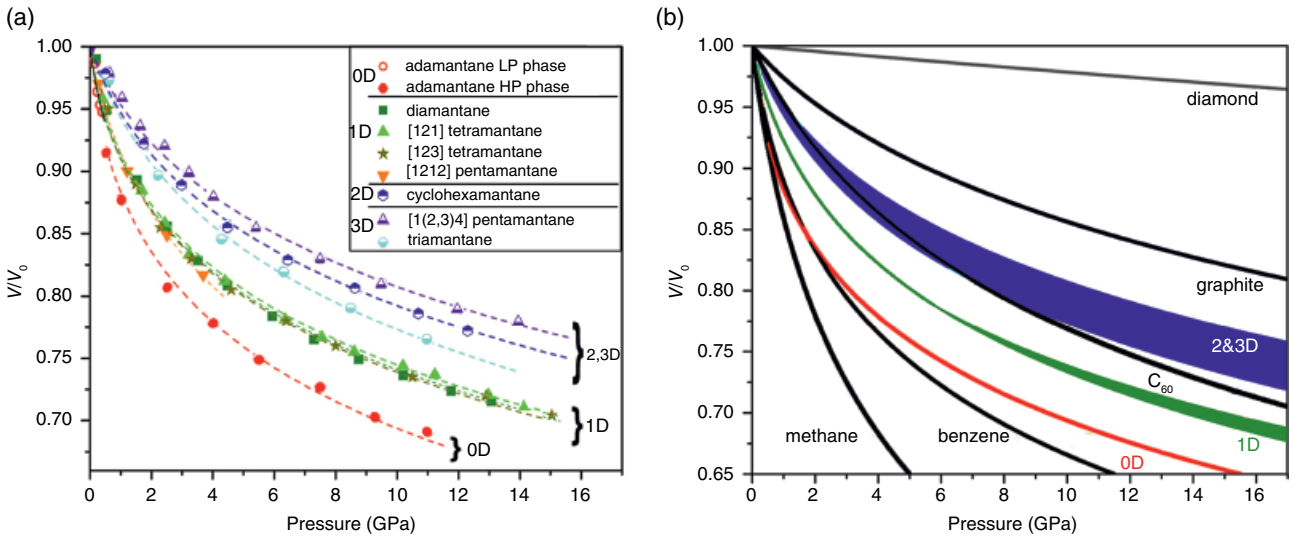

Figure 27.3 (a) Normalized unit cell volume changes as a function of increasing pressure in various diamondoid crystals. Dashed lines are pressure-volume curves fitted to the third-order Birch-Murnaghan equations of state (EOSs). (b) The EOS distributions of diamondoids categorized by the different dimensionalities. For comparisons, EOSs of other carbon allotropes and hydrocarbons are plotted. (Adapted from Yang et al., 2016.) See electronic version for color representation of the figures in this book.

compact, leading to quick buildup of repulsive forces. Hence, those with smaller H–H distances require less compression to trigger phase change, resulting in low phase-transition pressures. Contrarily, large H–H distances imply that a greater compression is needed to reach a critical transition point and prompt a phase transformation, as evidenced by high phase-transition pressure of triamantane, which has ~20% higher H–H distance (2.81 Å) compared with adamantane and [1(2,3)4]pentamantane (Yang et al., 2016).

In addition to the sensitivity to H–H distance, phase transitions in diamondoids exhibit a strong dependency on hydrostaticity. By subjecting diamantane ($C_{14}H_{20}$) to different pressure media at high pressure, it was found that its crystal structure is extremely sensitive to deviatoric stress (Yang et al., 2014a). Diamantane transforms almost immediately (~0.15 GPa) when external pressure is applied under nonhydrostatic conditions (Yang et al., 2014a). This transition pressure, when silicone oil is applied, is elevated to 7 GPa, which coincides with the hydrostatic limit of silicone oil (Klotz et al., 2009). Further experiments using helium as a pressure medium confirmed that the discrepancy in transition pressure is associated with the pressure medium quality, which underlines the critical role of deviatoric stress in triggering phase transitions in diamondoids (Yang et al., 2014a, 2014b). Indeed, deviatoric stress plays a critical role in inducing phase transformations, and in some cases, greatly reduces phase-transition pressure (Kailer et al., 1998; Y. Lin et al., 2011). Under hydrostatic conditions, diamondoids preserve their initial high-symmetry phases until the distortion of the unit-cell geometry becomes too high and eventually results in the observed phase changes.

Diamondoids are very robust in response to multiple rounds of compression and decompression. Even after 20 repeated pressure cycles up to ~5 GPa, diamondoids were able to retain their initial structures (Figure 27.4). This exquisite recoverability, combined with small ambient bulk moduli and high structural stability, makes diamondoids promising candidates for cushioning devices. In fact, diamondoids' recoverability far exceeds that of more conventional materials, such as foamy polystyrene and recently proposed carbon nanotube cushion materials (Liu et al., 2008). The energy absorption density (at ~2 GPa) of lower diamondoids is on the order of 10^2 kJ/kg, which is at least one order of magnitude greater than those of conventional cushion materials (Liu et al., 2008). In addition to possible applications in cushioning devices, the unique properties of diamondoids offer several other applications. For example, the geometry-dependent physical property of diamondoids suggest a possibility in designing nanoscale structures with tunable mechanical strength. The robust diamondoid networks also make them ideal materials to synthesize acentric metal-organic

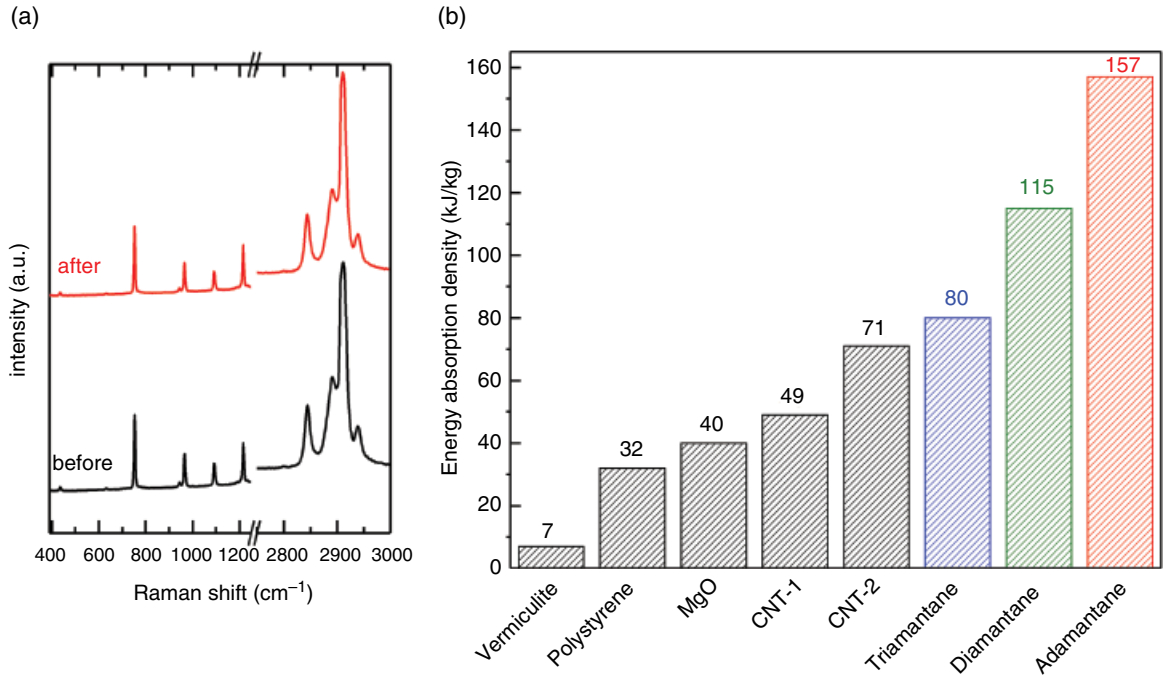

Figure 27.4 (a) Raman spectra of adamantane before and after 20 pressure cycles up to ~5 GPa. (b) Energy absorption density of conventional cushioning materials compared with three lower diamondoids. CNT-1 and CNT-2 refer to the microagglomerate and superagglomerate carbon nanotubes, respectively (Liu et al. 2008). (Reproduced from Yang et al. 2016.) See electronic version for color representation of the figures in this book.

diamondoid frameworks or supramolecular systems (Evans & Lin, 2001; Evans et al., 1999; Zaworotko, 1994).

27.3. CURRENT AND FUTURE PROSPECTS AND DIRECTIONS

Motivated by the unique properties of diamondoids, including their systematic sizes and geometries, a large body of work has recently been devoted to selectively separate, manipulate, and functionalize diamondoids (Gunawan et al., 2014). A wide range of functionalized diamondoid molecules have been reported with great potential for applications in molecular electronics, mechanics, biology, and chemistry (e.g. Archibald et al., 1991; Malik et al., 1991; Mcintosh et al., 2004; Patel et al., 2008; Shinisha & Sunoj 2005; Tewari et al., 2005; Wang et al., 2011). These studies take advantage of the fact that diamondoids are excellent building blocks to construct complex ordered nanoelements with molecular precision for their superior stability and rigidity (Garcia et al., 2009; Gunawan et al., 2014; Merkle, 2000). However, the diamondoid units on their own can be brittle due to full hybridization with hydrogen and weak intermolecular interactions (Garcia et al., 2009, Yan et al., 2018). Functionalization of such diamondoid molecules aims to solve several of the limitations by generating chemically active sites and manipulating the intermolecular/intramolecular interactions for fine tuning of the nanostructures. Such functionalization encourages self-assembly of the building blocks, eventually driving the system to optimized configurations (Garcia et al., 2009).

Recently, novel mechanochemistry through isotropic compression by engineering molecular structures that translate macroscopic isotropic stress into molecular-level anisotropic strain was reported (Yan et al., 2018). The "steric blockage" scenario, where rigid ligands in steric contact hampers relative motion and hinders reactivity, is demonstrated using copper(1) adamantane-1-thiolate (Cu-S-Ada), which is proposed for mechanochemistry of specific mechanosynthesis (Yan et al., 2018).

Cu-S-Ada crystals are composed of the mechanophore, a Cu-S nanowire, with a three-atom cross-section that is surrounded by a ligand shell consisting of adamantyl groups (Figure 27.5) (Yan et al., 2017; Yan et al., 2018). The sterically hindered ligand shell of Cu-S-Ada, caused by the rigid ligands, impedes relative movement of the adamantyl groups and deformation of Cu-S mechanophore. Density functional theory calculations show that the structure of adamantyl groups in Cu-S-Ada crystals remains rigid up to 20 GPa with less than 0.01 Å change in the average C-C bond length (Yan et al., 2018). Upon pressure release, the initial structure is recovered, indicating that the deformation is elastic. Such results are vastly dissimilar to the comparable building block system of copper(1) *m*-carborane-9-thiolate (Cu-S-M9) crystals (where *m* = meta positions of the carbon atoms in the carborane), wherein the cage-like nature and substantially large molecular distance between the M9 groups enable relatively free motions without mutual steric hindrance under compression (Yan et al., 2018). The free motions of Cu-S-M9 leads to a reduction of copper (Cu[1] → Cu[0]) after compression up to ~8 GPa, driven by the anisotropic deformation of Cu_4S_4 core (Yan et al., 2018). This reduction process, however, is inhibited when adamantane replaces the main building block, and the sterically hindered ligands limit the density differences near mechanophore, prohibiting any chemical reaction to occur (Yan et al., 2018).

The possible mechanochemistry driven by the relative motion of the rigid ligands of diamondoid cages functionalized with transition metals and chalcogens opens further exciting avenues for highly specific mechanosynthesis. The behavior of specific properties tuned from the functionalization of diamondoids should be further constrained by investigating the physical and chemical evolution under extreme conditions.

The exceptional properties of diamondoids and functionalized diamondoids point towards many potential applications. As discussed above, the stability of diamondoids in response to repeated pressure cycling makes them attractive candidates for cushioning devices.

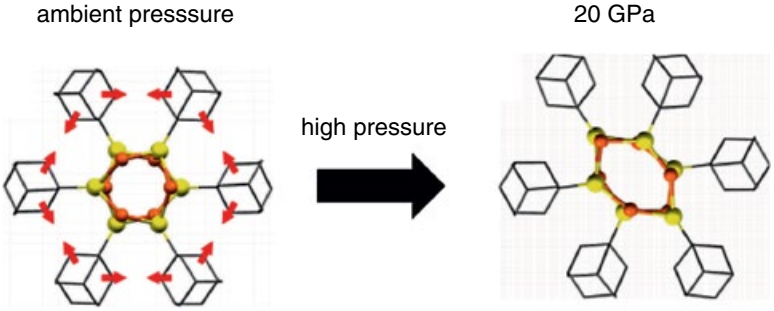

Figure 27.5 Structure of Cu-S-Ada crystals at ambient conditions. Red arrows denote the direction of motion for adamantyl groups under compression. (Reproduced from Yan et al., 2018.) See electronic version for color representation of the figures in this book.

Furthermore, rigid ligands from molecular engineering and functionalization diamondoids make them attractive for mechanochemistry and mechanosynthesis.

The evolution of structures and properties in diamondoid molecules upon compression warrants further investigations involving additional stimuli, such as high temperature. The simultaneous exposure of diamondoids to static high pressure and temperature could potentially cause spontaneous dehydrogenation, which in turn could drive the materials to form novel phases or unique structures not easily accessible using alternative pathways or precursor systems. A potential outcome of this is diamond. Given the resemblance of the diamondoids to the bulk diamond, diamondoid molecules may serve as optimal seed materials for forming diamond at high pressure and temperature. Additionally, time-resolved studies can be conducted to visualize the melting and reconstruction of shock-compressed diamondoids. Such studies can be performed by coupling the extremely bright X-ray pulses from X-ray free-electron lasers like the Linac Coherent Light Source (LCLS) at SLAC National Accelerator Laboratory with a high power optical laser, which can generate a shockwave in the material that results in high-pressure/high-temperature conditions. By probing material modifications in a nanosecond time regime, the dynamic pathways driving transitions in diamondoids can be evaluated, including the intermediate state that may not be accessible through static compression. These results will not only provide insight into the transformation of hydrocarbons into diamond or other carbon allotropes, but also help in determining physical and chemical parameters for synthesizing desirable carbon phases.

ACKNOWLEDGMENTS

The static compression experimental work was supported by the Department of Energy under Contract DE-AC02-76SF00515. The computational work and ongoing dynamic compression experiments are supported by the National Science Foundation under award ECCS-1542152, as well as the Deep Carbon Observatory.

REFERENCES

Archibald, T. G., Malik A. A., Baum, K. and Unroe, M. R (1991). Thermally stable acetylenic adamantane polymers. *Macromolecules*, *24*(19), 5261–5265.

Birch, F. (1947). Finite elastic strain of cubic crystals. *Physical Review*, *71*(11), 809–824.

Clay, W. A., Liu, Z., Liu, Z., Yang, W., Fabbri, J. D., et al. (2009). Origin of the monochromatic photoemission peak in diamondoid monolayers. *Nano Letters*, *9*(1), 57–61. doi:10.1021/nl802310k

Dahl, J. E., Liu, S. G., & Carlson, R.M.K. (2003). Isolation and structure of higher diamondoids, nanometer-sized diamond molecules. *Science*, 299(5603), 96–99. doi:10.1126/science.1078239

Dahl, J.E.P., Moldowan, J. M., Peters, K E., Claypool, G. E., Rooney, M. A., Michael, G. E., et al. (1999). Diamondoid hydrocarbons as indicators of natural oil cracking. *Nature*, *399*, 54–57. doi:10.1038/19953

Dahl, J.E.P., Moldowan, J. M., Wei, Z., Lipton, P. A., et al. (2010). Synthesis of higher diamondoids and implications for their formation in petroleum. *Angew. Chem. Int. Ed.*, *49*, 9881–9885. doi:10.1002/anie.201004276

Ekweozor, C. M., & Telnaes, N. (1990). Oleanane parameter: Verification by quantitative study of the biomarker occurrence in sediments of the Niger Delta. *Organic Geochemistry*, *16*(1-3), 401–413. doi:10.1016/0146-6380(90)90057-7

Evans, O. R, & Lin, W. (2001). Crystal engineering of nonlinear optical materials based on interpenetrated diamondoid coordination networks. *Chem Mater*, *13*, 2705–2712. doi:10.1021/cm010301n

Evans, O. R., Xiong, R.-G., Wang, Z.-Y., Wong, G. K., & Lin, W. (1999). Crystal engineering of acentric diamondoid metal-organic coordination networks. *Angew. Chem. Int. Ed.*, *38*(4), 536–538.

Filik, J., Harvey, J. N., Allan, N. L., May, P. W., Dahl, J.E.P., Liu, S., & Carlson, R. M. K. (2006). Raman spectroscopy of diamondoids. *Spectrochimica Acta Part A: Molecular and Biomolecular Spectroscopy*, *64*(3), 681–692. doi:10.1016/j.saa.2005.07.070

Filik, J., Harvey, J. N., Allan, N. L., May, P. W., Dahl, J.E.P., Liu, S., & Carlson, R. M. K. (2006). Raman spectroscopy of nanocrystalline diamond: An ab initio approach. *Physical Review B*, *74*(035423). doi:10.1103/PhysRevB.74.035423

Filik, J. (2010). Diamondoid hydrocarbons. In N. Ali, A. Öchsner, & W. Ahmed (Eds.), *Carbon-based nanomaterials* (chap. 1). Zurich; Enfield, NH: Trans Tech Publications. http://www.academia.edu/495358/Diamondoid_Hydrocarbons

Fort, R. C. Jr., & Schleyer, P.V.R. (1964). Adamantane: Consequences of the diamondoid structure. *Chem. Rev.*, *64*, 277–300.

Garcia, J. C., Justo, J. F., Machado, W.V.M., & Assali, L.V.C. (2009). Functionalized adamantane: Building blocks for nanostructure self-assembly. *Physical Review B*, *80*(125421). doi:10.1103/PhysRevB.80.125421

Gunawan, M. A., Hierso, J. C., Poinsot, D., Fokin, A. A., Fokina, N. A., Tkachenko, B. A., and Schreiner, P. R. (2014). Diamondoids: Functionalization and subsequent applications of perfectly defined molecular cage hydrocarbons. *New J. Chem*, *38*, 28–41. doi:10.1039/c3nj00535f.

Kailer, A., Gogotsi, Y G., & Nickel. K. G. (1998). Phase transformations of silicon caused by contact loading. *Journal of Applied Physics*, *81*(7), 3057–3063. doi:10.1063/1.364340

Katz, B. J., Mancini, E. A., & Kitchka, A. A. (2008). A review and technical summary of the AAPG Hedberg Research Conference on "Origin of petroleum—Biogenic and/or abiogenic and its significance in hydrocarbon exploration and production. *AAPG Bulletin*, *92*(5), 549–556. doi:10.1306/01210808006

Klotz, S., Chervin, J-C., Munsch, P., & Marchand, G. L. (2009). Hydrostatic limits of 11 pressure transmitting media. *Journal*

of Physics D: Applied Physics, *42*(7), 075413. doi:10.1088/0022-3727/42/7/075413

Lin, R., & Wilk. Z. A. (1995). Natural occurrence of tetramantane (C22H28), pentamantane (C26H32) and hexamantane (C30H36) in a deep petroleum reservoir. *Fuel*, *74*(10), 1512–1521.

Lin, Y., Yang, Y., Ma, H. W., Cui, Y., & Mao, W. L. (2011). Compressional behavior of bulk and nanorod LiMn 2 O 4 under nonhydrostatic stress. *J. Phys. Chem. C*, *115*, 9844–9849. doi:10.1021/jp112289h

Liu, Y., Qian, W., Zhang, Q., Cao, A., Li, Z., Zhou, W., et al. (2008). Hierarchical agglomerates of carbon nanotubes as high-pressure cushions. *Nano Letters*, *8*(5), 1323–1327. doi:10.1021/nl0733785

Ma, A. (2016). Advancement in application of diamondoids on organic geochemistry. *Journal of Natural Gas Geoscience*, *1*(4), 257–265. doi:10.1016/J.JNGGS.2016.09.001

Ma, A., Jin, Z., Zhu, C., & Bai, Z. (2017). Cracking and thermal maturity of Ordovician oils from Tahe Oilfield, Tarim Basin, NW China. *Journal of Natural Gas Geoscience*, *2*(4), 239–252. doi:10.1016/J.JNGGS.2017.12.001

Mackenzie, A. S., Patience, R. L., Maxwell, J. R., Vandenbroucke, M., & Durand, B. (1980). Molecular parameters of maturation in the Toarcian Shales, Paris Basin, France: I. Changes in the configurations of acyclic isoprenoid alkanes, steranes and triterpanes. *Geochimica et Cosmochimica Acta*, *44*(11), 1709–1721. doi:10.1016/0016-7037(80)90222-7

Malik, A. A., Archibald, R. G., Baum, K., & Unroe, M. R. (1991). New high-temperature polymers based on diamantane. *Macromolecules*, *24*, 5266–5268.

Mansoori, G. A. (2008). Diamondoid molecules. *Advances in Chemical Physics*, *136*, 207–58. doi:10.1002/9780470175422.ch4

Marchand, A. P. (2003). Diamondoid hydrocarbon: Delving into nature's bounty. *Science*, *299*(5603), 52–53. doi:10.1126/science.1078239

Mcintosh, G. C, Yoon, M., Berber, S., & Tománek, D. (2004). Diamond fragments as building blocks of functional nanostructures. *Physical Review*, *70*(045401). doi:10.1103/PhysRevB.70.045401

Mckervey, M. A. (1980). Synthetic approaches to large diamondoid hydrocarbons. *Tetrahedron*, *36*(8), 971–992. doi:10.1016/0040-4020(80)80050-0

Merkle, R. C. (2000). Molecular building blocks and development strategies for molecular nanotechnology. *Nanotechnology*, *11*, 89–99.

Patel, K., Angelos, S., Dichtel, W. R., Coskun, A., Yang, Y.-W., Zink, J. I., & Stoddart, J. F. (2008). Enzyme-responsive snap-top covered silica nanocontainers. *Jour. Amer. Chem. Soc.*, *130*, 2382–83. doi:10.1021/ja0772086

Requejo, A. G., Gray, N. R., Freund, H., Thomann, H., Melchior, M. R., Gebhard, L. A., et al. (1992). Maturation of petroleum source rocks: 1. Changes in kerogen structure and composition associated with hydrocarbon generation. *Energy & Fuels*, *6*(2), 203–214. doi:10.1021/ef00032a015

Sasagawa, R., Shen, Z-X. (2008). A route to tunable direct band-gap diamond devices: Electronic structures of nanodiamond crystals. *Journal of Applied Physics*, *104*(7), 073704. doi:10.1063/1.2986637

Seifert, W. K., & Moldowan, J. M. (1986). Use of biological markers in petroleum exploration. *Meth. in Geochem. and Geophy.*, *24*, 261–290.

Shinisha, C. B., & Sunoj, R. B. (2005). On the origins of kinetic resolution of cyclohexane-1,2-diols through stereoselective acylation by chiral tetrapeptides. *Tetrahedron: Asymmetry*, *44*(2), 3242–3245. doi:10.1021/ol9011822

Stauss, S., & Terashima, K. (2017). *Diamondoids: Synthesis, Properties and applications*, 1st ed. CRC Press.

Stout, S. A., & Douglas. G. S. (2004). Diamondoid hydrocarbons: Application in the chemical fingerprinting of natural gas condensate and gasoline. *Environmental Forensics*, *5*(4), 225–235. doi:10.1080/15275920490886734

Tewari, A., Hein, M., Zapf, A., & Beller, M. (2005). Efficient palladium catalysts for the amination of aryl chlorides: A comparative study on the use of phosphium salts as precursors to bulky, electron-rich phosphines. *Tetrahedron*, *61*(41), 9705–9709. doi:10.1016/J.TET.2005.06.067

Van Gass, G. W. (1990). Biomarker maturity parameters for high maturities: Calibration of the working range up to the oil/condensate threshold. *Org. Geochem.*, *16*(4-6), 1025–1032.

Wang, Y., Tkachenko, B. A., Schreiner, P. R., & Marx. A. (2011). Diamondoid-modified DNA. *Org. Biomol. Chem*, *9*(7482). doi:10.1039/c1ob05929g

Willey, T. M., Bostedt, C., Buuren, T. V., Dahl, J.E.P., Liu, S. G., Carlson, R.M.K., et al. (2006). Observation of quantum confinement in the occupied states of diamond clusters. *Physical Review B*, *74*(205432). doi:10.1103/PhysRevB.74.205432

Wingert, W. S. (1992). G.c.-m.s. analysis of diamondoid hydrocarbons in smackover petroleums. *Fuel*, *71*(1), 37–43. doi:10.1016/0016-2361(92)90190-Y

Yan, H., Hohman, J. N., Li, F. H., Jia, C. J., Solis-Ibarra, D., Wu, B., et al. (2017). Hybrid metal–organic chalcogenide nanowires with electrically conductive inorganic core through diamondoid-directed assembly. *Nature Materials*, *16*(3), 349–355. doi:10.1038/nmat4823

Yan, H., Yang, F., Pan, D., Lin, Y., Hohman, J. N., Solis-Ibarra, D., Li, H. et al. (2018). Sterically controlled mechanochemistry under hydrostatic pressure. *Nature*, *554*, 505–510. doi:10.1038/nature25765

Yang, F., Lin, Y., Baldini, M., Dahl, J.E.P., Carlson, R.M.K., & Mao, W. L. (2016). Effects of molecular geometry on the properties of compressed diamondoid crystals. *J. Phys. Chem. Lett*, *7*, 4641–4647. doi:10.1021/acs.jpclett.6b02161

Yang, F., Lin, Y., Dahl, J.E.P., Carlson, R.M.K., & Mao, W. L. (2014a). Deviatoric stress-induced phase transitions in diamantane. *The Journal of Chemical Physics*, *141*(15), 154305. doi:10.1063/1.4897252

Yang, F., Lin, Y., Dahl, J.E.P., Carlson, R.M.K., & Mao, W. L. (2014b). High pressure Raman and X-ray diffraction study of [121] tetramantane. *The Journal of Physical Chemistry C*, *118*, 7683–7689. doi:10.1021/jp500431k

Zaworotko, M. J. (1994). Crystal engineering of diamondoid networks. *Chemical Society Reviews*, *23*(4), 283. doi:10.1039/cs9942300283

Zhang, J. L., Ishiwata, H., Babinec, T. M., Radulaski, M., Mü K., Lagoudakis, K. G., et al. (2016). Hybrid Group IV nanophotonic structures incorporating diamond silicon-vacancy color centers. *Nano Lett*, *16*, 212–217. doi:10.1021/acs.nanolett.5b03515